ISSN 1063-7737, Astronomy Letters, 2009, Vol. 35, No. 1, pp. 57–69. © Pleiades Publishing, Inc., 2009.
Original Russian Text © S.A. Bogachev, B.V. Somov, 2009, published in Pis'ma v Astronomicheskiĭ Zhurnal, 2009, Vol. 35, No. 1, pp. 63–75.

Effect of Coulomb Collisions on the Particle Acceleration in Collapsing Magnetic Traps

S. A. Bogachev[1]* and B. V. Somov[2]**

[1] *Lebedev Physical Institute, Russian Academy of Sciences, Leninskii pr. 53, Moscow, 119991 Russia*
[2] *Sternberg Astronomical Institute, Universitetskii pr. 13, Moscow, 119992 Russia*

Received January 31, 2008

Abstract—The problem of particle acceleration in collapsing magnetic traps in the solar corona has been solved by taking into account the particle scattering and braking in the high-temperature plasma of solar flares. The Coulomb collisions are shown to be weak in traps with lifetimes $t_l < 10$ s and strong for $t_l > 100$ s. In the approximation of strong collisions, collapsing magnetic traps are capable of confining up to 20% of the injected particles in the corona for a long time. In the collisionless approximation, this value exceeds 90%. The question about the observational manifestations of collisions is examined. For collision times comparable to t_l, the electron spectrum at energies above 10 keV is shown to be a double-power-law one. Such spectra were found by the RHESSI satellite in flares.

PACS numbers : 52.30.Cv; 94.05.-a; 95.30.Qd
DOI: 10.1134/S1063773709010071

Key words: *Sun, solar flares, magnetic reconnection, particle acceleration, X-ray emission.*

INTRODUCTION

The acceleration of charged particles in the solar corona during flares exhibits peculiarities some of which have no universally accepted explanation as yet (see, e.g., Miroshnichenko 2001). Particles with an initial energy of ~0.1 keV, corresponding to the coronal temperature, increase it to 10–100 keV and even to 10–100 MeV in very short times, from seconds to several tens of seconds. Heavy particles, ions, are accelerated with a higher efficiency (i.e., to higher energies) than electrons. The increase in particle energy is usually accompanied by a change in the shape of the particle energy spectrum. In a considerable number of flares, the appearance of higher-energy particles is delayed relative to that of lower-energy ones.

The listed peculiarities can be explained in terms of the model of a two-stage particle acceleration during flares with collapsing magnetic traps (Somov and Kosugi 1997; Bogachev and Somov 2001, 2005, 2007; Aschwanden 2002; Kovalev and Somov 2003; Somov and Bogachev 2003; Karlicky and Kosugi 2004; Giuliani et al. 2005). According to this model, the electrons and ions are initially accelerated in the magnetic reconnection region, in a high-temperature turbulent current sheet (HTTCS; Somov 2006a, 2006b). Here, the electrons can be accelerated at least to 10 keV (i.e., to an energy that corresponds to the HTTCS electron temperature). After their escape from the HTTCS, the particles are captured into collapsing magnetic traps formed by reconnected magnetic field lines whose footpoints are located in the chromosphere. The longitudinal and transverse sizes of the traps decrease during flares, causing the trapped particles to acquire an additional energy under Fermi and betatron accelerations. This is the second stage of particle acceleration. Characteristically, the protons are accelerated during this stage to higher energies than the electrons (Somov et al. 2002).

Interacting with one another, the particles inside a trap produce X-ray bremsstrahlung whose sources are observed in the corona during flares. The locations of the sources (above the flare loops) coincide with the places of particle trapping and acceleration. The main types of coronal X-ray spectra can also be explained in terms of the model under consideration (Bogachev and Somov 2007). The emission sources with a power-law spectrum are formed in traps when electrons with a power-law distribution are injected into them, irrespective of the dominant acceleration mechanism, the betatron or Fermi one. However, if the injection spectrum is thermal (and such electrons are always present in the HTTCS model), then it becomes a power law in traps with Fermi acceleration

*E-mail: bogachev@sci.lebedev.ru
**E-mail: somov@sai.msu.ru

and quasi-thermal with a very high temperature in traps with dominant betatron acceleration.

In this paper, we investigate the effect of Coulomb collisions on the efficiency of particle confinement and acceleration in a trap and on the shape of the particle spectrum. This formulation of the problem, including the scattering of particles and the losses of their energy as they brake in the background plasma, corresponds to the actual physical conditions in the corona and, hence, describes more accurately the dynamics of trapped particles than the collisionless approximation considered previously. The results of our calculations are compared with the formulas derived in the collisionless approximation, in which the problem of particle motion in a collapsing magnetic trap has relatively simple analytic solutions (Bogachev and Somov 2001, 2007).

QUALITATIVE DESCRIPTION OF THE EXPECTED EFFECT

In the collisionless approximation, which is applicable for electrons and ions with velocities much higher than the thermal velocity, only two factors affect the motion of trapped particles—Fermi and betatron accelerations in a collapsing magnetic trap. Let us consider the actual situation more carefully. The electrons and ions in a trap do not move freely but interact with one another and with the "background" plasma, i.e., the plasma formed by electrons and ions with velocities close to the thermal ones. Although these effects result from the action of Coulomb forces, we will distinguish them based on the following considerations. Elastic interactions between particles do not change their total energy but redistribute it between slow and fast particles. In addition, collisions result in particle scattering, which leads to particle diffusion in pitch angle. This is of fundamental importance for our analysis of the efficiency of the acceleration mechanisms given below.

Naturally, it does not follow from the conservation of the total kinetic energy of two particles as they collide elastically that scattering does not affect the acceleration efficiency in the trap. Previously (Bogachev and Somov 2005), we showed in the collisionless approximation that, irrespective of the acceleration mechanism (betatron, Fermi, or both), the ratio of the final particle energy, $K_{\rm esc}$, to the initial one, K_0, is defined by the formula

$$K_{\rm esc}/K_0 = b_{\rm m}\sin^2\alpha. \quad (1)$$

Here, α is the particle pitch angle and $b_{\rm m}$ is the initial mirror ratio, i.e., the ratio of the magnetic field in the magnetic mirrors, $B_{\rm m}$, to the initial field at the trap center, B_0:

$$b_{\rm m} = B_{\rm m}/B_0. \quad (2)$$

It thus follows that if the particles are scattered in the direction of large pitch angles ($\alpha \to \pi/2$), then their final energy $K_{\rm esc}$ increases, although the energy K_0 remains constant. Similarly, diffusion in the direction of small pitch angles ($\alpha \to 0$) reduces the acceleration efficiency. The preferential direction of the pitch-angle diffusion depends on the particle pitch-angle distribution and can be different at different trap collapse stages and in different segments of the pitch-angle distribution and the energy spectrum.

Generally, when particular acceleration mechanisms in cosmic plasmas are considered, the role of Coulomb collisions is reduced to the energy losses of the accelerated particles, in particular, to the presence of a "loss barrier" at low velocities (see, e.g., Korchak 1980; Bykov et al. 2000). As a result, collisions are believed to reduce the efficiency of any acceleration mechanism. Meanwhile, it follows from general principles (see Somov 2006b, Section 12.3) that weak collisions between the accelerated electrons in collapsing magnetic traps, which cause their isotropization, increase the phase space volume of the particles involved in the acceleration process. Thus, in general, the electron acceleration efficiency in collapsing magnetic traps can be increased significantly (Kovalev and Somov 2003). We are interested in the question of precisely how this effect is realized in collapsing magnetic traps of solar flares.

FORMULATION OF THE PROBLEM OF NUMERICAL SIMULATION

We will use the method of numerical simulation described below to solve the problem of the effect of Coulomb collisions on the particle acceleration in a collapsing magnetic trap. We will describe a particle by two parameters, its kinetic energy K and pitch angle α, and investigate their variations. We are not interested in the question of precisely where the particle is located inside the trap at each time. This approach differs from the standard methods based on the numerical integration of the equations of motion for many interacting particles.

What factors change the energy K and pitch angle α of a trapped particle? These primarily include the betatron and Fermi accelerations, the scattering and braking of particles in the background plasma, their acceleration and braking by an electric field, and other factors that can be significant under particular conditions (see Somov 2006a). Let us write their combined effect on K and α using the functions F_k and F_α in the form of the equations

$$\frac{dK}{d\tau} = F_k(K,\alpha,\tau), \quad \frac{d\alpha}{d\tau} = F_\alpha(K,\alpha,\tau). \quad (3)$$

Here, τ is a generalized time, i.e., in general, any variable whose monotonic change determines the dynamics of the process. When traps with a decreasing length L are investigated, it is convenient to use the dimensionless trap length $l = L/L_0$, which changes from 1 to 0, as the generalized time. For transversally collapsing traps, this can be the parameter $b = B/B_0$, which changes from 1 to b_m and characterizes the degree of magnetic field compression. Naturally, the physical time t normalized to the unit of measurement can also be meant by τ.

The essence of our numerical model consists in the following. We consider an arbitrary time τ and assume that the distribution of trapped particles in pitch angle and energy at this time is described by a function $f(K,\alpha)$. This function is known. It is specified by the initial conditions at the initial time and is determined numerically from the preceding evolutionary stages at τ. Let us now shift by a short time interval $\Delta\tau$ and introduce an unknown function $f_1(K_1,\alpha_1)$, the distribution of trapped particles at the time $\tau+\Delta\tau$. We will link the two distributions using the transformation Jacobian $\mathcal{P}$:

$$2\pi f_1(K_1,\alpha_1)\sqrt{K_1}\sin\alpha_1\mathcal{P} = 2\pi f(K,\alpha)\sqrt{K}\sin\alpha. \quad (4)$$

Here, K and α are the particle energy and pitch angle at τ, while K_1 and α_1 are the particle energy and pitch angle at τ_1. According to Eqs. (3), these are related by

$$K_1 = K + F_k\Delta\tau, \quad \alpha_1 = \alpha + F_\alpha\Delta\tau. \quad (5)$$

Using Eqs. (5), let us calculate the Jacobian

$$\mathcal{P} = \begin{pmatrix} \frac{\partial\alpha_1}{\partial\alpha} & \frac{\partial K_1}{\partial\alpha} \\ \frac{\partial\alpha_1}{\partial K} & \frac{\partial K_1}{\partial K} \end{pmatrix} = \begin{pmatrix} 1+\frac{\partial F_\alpha}{\partial\alpha}\Delta\tau & \frac{\partial F_k}{\partial\alpha}\Delta\tau \\ \frac{\partial F_\alpha}{\partial K}\Delta\tau & 1+\frac{\partial F_k}{\partial K}\Delta\tau \end{pmatrix}.$$

Once the terms have been grouped by orders of smallness in $\Delta\tau$, we have

$$\mathcal{P} = 1 + D_1\Delta\tau + D_2\Delta\tau^2, \quad (6)$$

where the coefficients

$$D_1 = \left(\frac{\partial F_\alpha}{\partial\alpha} + \frac{\partial F_k}{\partial K}\right), \quad (7)$$
$$D_2 = \left(\frac{\partial F_\alpha}{\partial\alpha}\frac{\partial F_k}{\partial K} + \frac{\partial F_\alpha}{\partial K}\frac{\partial F_k}{\partial\alpha}\right).$$

Let us now return to Eq. (4) and expand the distribution $f_1(K_1,\alpha_1)$ in terms of the small parameter $\Delta\tau$:

$$f_1(K_1,\alpha_1) = f_1(\alpha,K) + \left(\frac{\partial f_1}{\partial\alpha}\right)F_\alpha\Delta\tau + \left(\frac{\partial f_1}{\partial K}\right)F_k\Delta\tau. \quad (8)$$

Similarly, let us transform the factors $\sin\alpha_1$ and $\sqrt{K_1}$ appearing in (4):

$$\sin\alpha_1 = \sin\alpha + \cos\alpha F_\alpha\Delta\tau \quad (9)$$

and

$$\sqrt{K_1} = \sqrt{K} + \frac{1}{2\sqrt{K}}F_k\Delta\tau. \quad (10)$$

Substituting Eqs. (6), (8), (9), and (10) into (4) yields the equation

$$f(K,\alpha) = \left[f_1(\alpha,K) + \left(\frac{\partial f_1}{\partial\alpha}\right)F_\alpha\Delta\tau + \left(\frac{\partial f_1}{\partial K}\right)F_k\Delta\tau\right]\left(1+\frac{F_\alpha}{\tan\alpha}\Delta\tau\right) \times\left(1+\frac{F_k}{2K}\Delta\tau\right)\left(1+D_1\Delta\tau+D_2\Delta\tau^2\right). \quad (11)$$

Recall that the function $f(K,\alpha)$ is assumed to be known, while the function $f_1(\alpha,K)$ is unknown. Since the distribution f_1 appears on the right-hand side of Eq. (11) together with its derivatives with respect to the pitch angle and energy, the derived equation is not closed. Note, however, that the functions f_1 and f differ by a quantity of the first order of smallness in $\Delta\tau$:

$$f_1 = f + o(\Delta\tau). \quad (12)$$

This means that disregarding the terms of the second order of smallness, we can substitute $\partial f/\partial\alpha$ and $\partial f/\partial K$, respectively, for the derivatives $\partial f_1/\partial\alpha$ and $\partial f_1/\partial K$ on the right-hand side of Eq. (11). After the substitution, we obtain

$$f_1 = \left[\left(1+\frac{F_\alpha}{\tan\alpha}\Delta\tau\right)\left(1+\frac{F_k}{2K}\Delta\tau\right) \times\left(1+D_1\Delta\tau+D_2\Delta\tau^2\right)\right]^{-1} f - \left[\left(\frac{\partial f}{\partial\alpha}\right)F_\alpha + \left(\frac{\partial f}{\partial K}\right)F_k\right]\Delta\tau. \quad (13)$$

Formula (13) is defined to terms of the second order of smallness in $\Delta\tau$. If we use f_1 found in this way to calculate the derivatives $\partial f_1/\partial\alpha$ and $\partial f_1/\partial K$ on the right-hand side of Eq. (11) and repeat the calculations, then the result will be accurate to the third order of smallness in $\Delta\tau$ and so on.

If the time step $\Delta\tau$ is small compared to the characteristic times of the processes being studied, then the terms of all orders of smallness in $\Delta\tau$, except for the first order, may be neglected when f_1 is

determined. In this case, Eq. (13) can be simplified significantly:

$$\Delta f = -\left(\frac{F_\alpha}{\tan\alpha}f + \frac{F_k}{2K}f + \frac{\partial}{\partial\alpha}fF_\alpha + \frac{\partial}{\partial K}fF_k\right)\Delta\tau. \quad (14)$$

SIMULATION OF THE ACCELERATION PROCESSES

Equations (13) and (14) allow us to calculate how the distribution of trapped particles $f(K,\alpha)$ changes as the trap collapses. Let us first determine the ranges within which the pitch angle α and energy K vary. If a symmetric collapsing trap is considered, then the pitch angle ranges from 0 to $\pi/2$. In general, the kinetic energy can take on any values, although it rarely exceeds 100 MeV in the solar corona for the electrons accelerated in flares. Let us introduce a two-dimensional grid whose points are specified by the formulas

$$\alpha_i = \frac{\pi}{2}\frac{i}{N-1}, \quad K_j = 10^{-2+7j/(N-1)}\ \text{keV}, \quad (15)$$

where N is the grid size (in our calculations, $N = 1000$), while the indices i and j run from 0 to $N-1$.

Grid (15) uniformly covers the range of pitch angles from 0 to $\pi/2$ with a step $\Delta\alpha_i = (\pi/2)/(N-1)$ and the range of energies from 0.01 keV to 100 MeV. The step ΔK_j increases with $\mathcal{K}$. This allows the distribution of particles at low energies, where the bulk of them are located, to be investigated more accurately.

Before the beginning of our calculations, we should specify the values of $f_{ij} = f(K_j,\alpha_i)$ defining the initial particle distribution at the grid points. Except for the specially stipulated cases, this distribution will be assumed to be thermal and isotropic:

$$f_{ij} = \frac{1}{4\pi}\frac{2}{\sqrt{\pi k^3 T^3}}\exp\left(-\frac{K_j}{kT}\right). \quad (16)$$

If it is necessary to abandon this assumption, then it will suffice to replace the initial values at the grid points with new ones.

Fermi Acceleration

Before turning to the simulation of specific acceleration mechanisms, we will note that the general formula (13) shows how the distribution f at the time τ is transformed into the distribution f_1 at the time $\tau+\Delta\tau$. Naturally, it imposes no constraints on the factors under which this transformation is made. An unambiguous determination of these factors will suffice.

To apply Eq. (13) for a specific physical process, we must specify the functions F_α, F_k and the coefficients D_1, D_2. Let us begin our investigation with Fermi acceleration. In this case (Bogachev and Somov 2005), the particle pitch angle and energy in a trap change as

$$\tan\alpha = l\tan\alpha_0, \quad K = K_0\left(\frac{\cos^2\alpha_0}{l^2} + \sin^2\alpha_0\right), \quad (17)$$

where l is the dimensionless trap length that decreases from 1 to 0. Let us choose l as the generalized time. Having determined $\tau \equiv l$ in Eqs. (3), we find

$$F_\alpha = \frac{d\alpha}{dl} = \frac{\sin 2\alpha}{2l}, \quad F_k = \frac{dK}{dl} = -\frac{2K\cos^2\alpha}{l}. \quad (18)$$

Thus, the problem of the numerical simulation of Fermi acceleration is completely defined and solvable, since the parameters D_1 and D_2 are expressed in terms of the functions F_α and F_k. According to Eqs. (7),

$$D_1 = -\frac{1}{l}, \quad D_2 = -\frac{2\cos^2\alpha\cos 2\alpha}{l^2}. \quad (19)$$

Substituting (18) into (14), we find that in the approximation including only the terms of the first order of smallness, the equation for the numerical simulation of Fermi acceleration is

$$\Delta f = \left(f - \frac{\sin 2\alpha}{2}\frac{\partial f}{\partial\alpha} + 2K\cos^2\alpha\frac{\partial f}{\partial K}\right)\frac{\Delta l}{l}. \quad (20)$$

Equation (20), among other things, allows the accuracy of the numerical method to be estimated. Let us transform the model distribution (denote it by f_n) into the number of particles in the trap,

$$N_n(l) = 2\pi N_0 \times \int_0^\infty\int_\infty^{\pi-\alpha_{\rm esc}} f_n(K,\alpha,l)\sqrt{K}dK\sin\alpha d\alpha, \quad (21)$$

and compare it with the exact formula (Bogachev and Somov 2005),

$$N(l) = N_0\frac{l\sqrt{b_{\rm m}-1}}{\sqrt{1+(b_{\rm m}-1)l^2}}. \quad (22)$$

The ratio N_n/N is plotted against the trap length in Fig. 1. We see that the results of our calculations agree with the exact formula to within <1% up to a time $l \sim 0.003$. At smaller l, the accuracy decreases rapidly for an obvious reason. According to (17), the kinetic energy of the trapped particles increases with decreasing l. This is the Fermi acceleration. At the

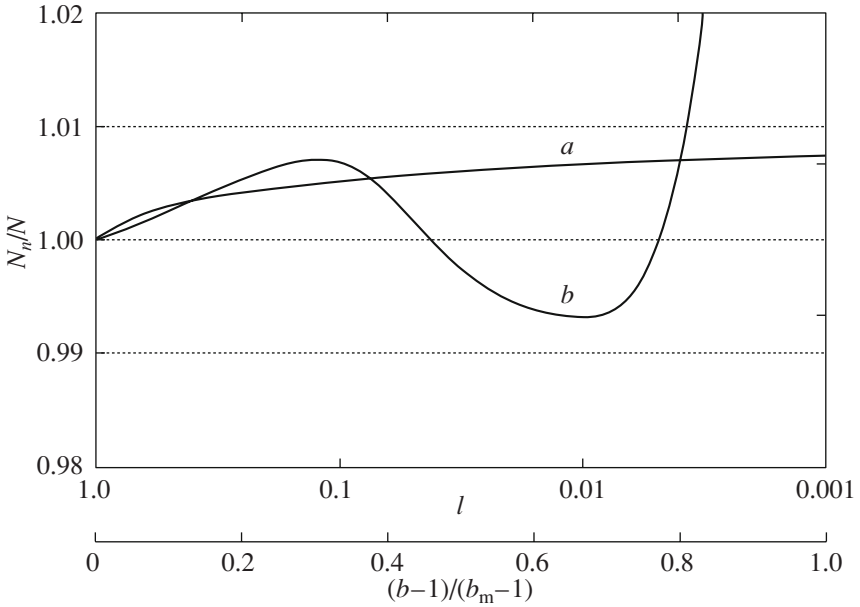

Fig. 1. Ratio of the numerically determined number of particles, N_n, to the exact number of particles N in a collapsing magnetic trap: a—betatron acceleration (N_n and N coincide to within $\sim 1\%$) and b—Fermi acceleration (the solutions coincide to within 1% up to a time $l \sim 0.003$).

final stage, when l approaches zero, K increases too rapidly to be described as a small increment within the interval Δl. This can be avoided by using a nonlinear time scale whose step decreases as $l \to 0$. However, we do not set the goal of investigating the particle dynamics at excessively low l, at which the physical processes disregarded in our simple model became significant, and we do not wish to complicate it by additional assumptions and features.

Betatron Acceleration

To simulate betatron acceleration, it is convenient to choose the dimensionless parameter b, which increases from 1 to b_m for a transversally collapsing trap, as the generalized time.

The particle pitch angle and kinetic energy for betatron acceleration change as

$$\tan\alpha = \sqrt{b}\tan\alpha, \quad K = K_0\left(\cos^2\alpha_0 + b\sin^2\alpha_0\right) \tag{23}$$

(Bogachev and Somov 2005). Having determined $\tau \equiv b$ in (3), we obtain

$$F_\alpha = \frac{\sin 2\alpha}{4b}, \quad F_k = \frac{K\sin^2\alpha}{b}. \tag{24}$$

According to (7), the coefficients

$$D_1 = \frac{1}{2b}, \quad D_2 = \frac{\sin^2\alpha\cos 2\alpha}{2b^2}. \tag{25}$$

Substituting (24) and (25) into Eq. (14) yields the following expression for betatron acceleration:

$$\Delta f = -\left(f + \frac{\sin 2\alpha}{4}\frac{\partial f}{\partial\alpha} + K\sin^2\alpha\frac{\partial f}{\partial K}\right)\frac{\Delta b}{b}. \tag{26}$$

In contrast to Fermi acceleration, the increase in particle energy for betatron acceleration is limited (see Eq. (23) for $b \to b_\mathrm{m}$). As a result, the numerical simulation of betatron acceleration is stable up to complete trap collapse, as demonstrated in Fig. 1.

COULOMB SCATTERING AND PARTICLE BRAKING

Recall that we distinguish two effects related to the Coulomb collisions between trapped particles inside a collapsing trap: the scattering of particles as they interact with one another and their braking in a high-temperature plasma (see the Section "Qualitative Description of the Expected Effect"). Let us first consider the first effect.

Particle Scattering

To take into account the Coulomb collisions, we will add the term containing the collision integral $(\partial f/\partial t)_\mathrm{c}$ to Eqs. (20) and (26), more specifically,

$$\Delta f_\mathrm{c} = \left(\frac{\partial f}{\partial t}\right)_\mathrm{c}\frac{\partial t}{\partial\tau}\Delta\tau. \tag{27}$$

Here, the factor $\partial t/\partial\tau$ relates the physical time t to the generalized time τ.

For traps with a decreasing length, as previously, we will set $\tau \equiv l$. In this case,

$$\frac{\partial t}{\partial \tau}\Delta\tau = \frac{\partial t}{\partial l}\Delta l = \frac{L_0}{\partial L/\partial t}\Delta l = -t_l\Delta l, \qquad (28)$$

where t_l is the characteristic time of the decrease in trap length. The minus arises, because $\partial L/\partial t < 0$.

For betatron acceleration at $\tau \equiv b$, we obtain

$$\frac{\partial t}{\partial \tau}\Delta\tau = \frac{\partial t}{\partial b}\Delta b \qquad (29)$$
$$= \frac{B_0}{B_\mathrm{m}-B_0}\frac{B_\mathrm{m}-B_0}{\partial B/\partial t}\Delta b = \frac{t_b}{b_\mathrm{m}-1}\Delta b.$$

The characteristic transverse collapse time, $\tan_\mathrm{b}$, determines how fast the initial magnetic field B_0 at the trap center becomes equal to the field B_m in the trap mirrors. In this case, the field increases by $B_\mathrm{m}-B_0$.

For the collision integral, we will use the simplest model

$$\left(\frac{\partial f}{\partial t}\right)_\mathrm{c} = \frac{f_\mathrm{M}-f}{t_\mathrm{c}}, \qquad (30)$$

which describes the relaxation of the current distribution $f(K,\alpha)$ to a Maxwellian one $f_\mathrm{M}(K,\alpha)$ under the action of Coulomb collisions. This simplification is admissible, since the time $\Delta\tau$ during which the interaction of particles is considered at each simulation step is short.

The characteristic relaxation time, t_c, is inversely proportional to the collision frequency and is

$$t_\mathrm{c} = \frac{\sqrt{m_e}K^{3/2}}{2\pi n_e e^4 \ln\Lambda}, \qquad (31)$$

where the Coulomb logarithm

$$\ln\Lambda = \ln\frac{3}{2e^3}\left(\frac{k^3T^3}{\pi n_e}\right)^{1/2}. \qquad (32)$$

The relaxation to a Maxwellian distribution proceeds with different speeds among particles of different energies. Low-energy particles are thermalized most rapidly. In contrast, the acceleration in the Maxwellian tail is almost collisionless. For particles with energies 10–100 keV at $n_p \approx 10^9$ cm^{-3}, the characteristic time t_c lies within the range 7–200 s. Moreover, the effect of Coulomb collisions decreases as the particles accelerate.

Substituting the collision integral (30) into Eqs. (20) and (26), we will find formulas to calculate the distribution function including the particle scattering. For Fermi acceleration, according to (27) and (28),

$$\Delta f_\mathrm{c} = -(f_\mathrm{M}-f)\left(\frac{t_l}{t_\mathrm{c}}\right)\Delta l, \qquad (33)$$

whence

$$\Delta f = \left(f - \frac{\sin 2\alpha}{2}\frac{\partial f}{\partial\alpha} + 2K\cos^2\alpha\frac{\partial f}{\partial K}\right)\frac{\Delta l}{l} \qquad (34)$$
$$-(f_\mathrm{M}-f)\frac{t_l}{t_\mathrm{c}}\Delta l.$$

For betatron acceleration,

$$\Delta f_\mathrm{c} = \frac{f_\mathrm{M}-f}{b_\mathrm{m}-1}\frac{t_\mathrm{b}}{t_\mathrm{c}}\Delta b. \qquad (35)$$

In this case,

$$\Delta f = -\left(f + \frac{\sin 2\alpha}{4}\frac{\partial f}{\partial\alpha}\right. \qquad (36)$$
$$\left. + K\sin^2\alpha\frac{\partial f}{\partial K}\right)\frac{\Delta b}{b} + \left(\frac{f_M-f}{b_\mathrm{m}-1}\right)\frac{t_\mathrm{b}}{t_\mathrm{c}}\Delta b.$$

The times t_l and t_b are determined by the trap properties in the corona. Different authors give different values for these times. Thus, for example, Brown and Hoyng (1975) considered the collisionless betatron acceleration of particles in a long-lived magnetic trap existing during the impulsive phase of a flare for ~1000 s. Traps with much shorter lifetimes were suggested by Somov and Kosugi (1997). They assumed the trap lifetimes to be determined by the time it takes for the reconnected magnetic field lines to move from the reconnection region (HTTCS) to the top of a stationary magnetic loop, a magnetic obstacle. As soon as the field line falls on this loop, the trap disappears. The lifetime of an individual trap was estimated by the authors to be 1–10 s. Having compared these lifetimes with the characteristic Coulomb collision time (7–200 s), we conclude that the collisions are weak in short-lived collapsing traps. To a first approximations, these may be neglected (Somov and Kosugi 1997; Bogachev and Somov 2001, 2005, 2007). In contrast, the particle acceleration in long-lived traps should be considered in the approximation of strong collisions.

Particle Braking in Plasma

Let us now consider the case where there is a background plasma together with energetic particles in the trap. This plasma can be injected from a current sheet together with particles or be located in the trap before injection.

Although the separation of matter into particles and plasma is somewhat arbitrary, it is justified in

many problems. The background plasma is often much denser and colder than the protons and electrons interacting with it and, therefore, forms a self-consistent MHD system whose properties differ from those of fast particles.

When simulating the particle acceleration in a trap with plasma, we will take into account the following effects: betatron acceleration, Fermi acceleration, escape through the loss cone, and relaxation in energy and pitch angle for plasma particles; all of the listed effects and energy losses through braking for fast particles.

To be specific, let us consider the Fermi acceleration of electrons. The equation for betatron acceleration can be derived similarly. Let us transform Eq. (34) in such a way that it includes the particle braking in plasma. For this purpose, we will use the well-known classical formula

$$\frac{dK}{dt} = -a\frac{n_p}{\sqrt{K}}, \quad a = \frac{e^4 \ln\Lambda}{4\sqrt{2m_e}}, \tag{37}$$

where n_p is the plasma proton density and $\ln\Lambda$ is the Coulomb logarithm. After transformations, we obtain

$$\frac{dK}{dl} = \frac{dK}{dt}\frac{dt}{dl} = a\frac{n_p}{\sqrt{K}}t_l. \tag{38}$$

Let us now return to the chain of Eqs. (18)–(20) and modify its first equation

$$F_k = \frac{dK}{dl} = -\frac{2K\cos^2\alpha}{l} + a\frac{n_p}{\sqrt{K}}t_l. \tag{39}$$

Repeating the calculations, we find

$$\Delta f = \left(f - \frac{\sin 2\alpha}{2}\frac{\partial f}{\partial \alpha} + 2K\cos^2\alpha\frac{\partial f}{\partial K}\right)\frac{\Delta l}{l} - \frac{an_p t_l}{\sqrt{K}}\left(\frac{\partial f}{\partial K} - \frac{1}{2K}f\right)\Delta l - (f_m - f)\frac{t_l}{t_c}\Delta l. \tag{40}$$

Here, the first, second, and third terms describe, respectively, the collisionless Fermi acceleration, the particle braking in plasma, and the scattering of particles as they interact with one another.

SIMULATION RESULTS

We now turn to the presentation of our simulation results. We will denote the numerically calculated distribution function by $f_n(K,\alpha)$. The subscript n distinguishes it from the exact function. Our main goal will be to compare the simulation results with the formulas derived in the collisionless approximation. This gives an insight into the extent to which the collisions between particles affect the efficiency of their acceleration in collapsing magnetic traps and the shape of their spectrum.

We will begin with an analysis of the pitch-angle distribution:

$$f_n(\alpha) = \int_0^\infty f_n(K,\alpha)\sqrt{K}dK. \tag{41}$$

In collapsing traps with lifetimes shorter than 10 s, Coulomb scattering affects only slightly the particle pitch-angle distribution. In long-lived traps with lifetimes of ~1000 s, the role of scattering is more significant. The results of our calculations for this case are shown in Fig. 2.

Curve *a* in both figures indicates the initial particle pitch-angle distribution, which was assumed to be isotropic. As the trap collapses, this distribution is modified. In the collisionless approximation, as we showed previously (Bogachev and Somov 2005), it changes as

$$F_\alpha a = \frac{1}{4\pi}\frac{l\sqrt{b}}{\left(\sin^2\alpha + bl^2\cos^2\alpha\right)^{3/2}} \tag{42}$$

and takes the shape *b* and, in the approximation with Coulomb particle scattering, the shape *c*. The difference between curves *b* and *c* shows the difference between the two cases. As would be expected, the interaction of particles causes isotropization of their pitch-angle distribution. As a result, the latter is intermediate between two limits — the collisionless and isotropic ones. The stronger the interaction, the closer the distribution to the isotropic limit.

If we select a sector of pitch angles $[\alpha, \alpha + d\alpha]$ in the pitch-angle distribution, then the number of particles in the sector can both increase and decrease compared to the collisionless case as a result of their scattering. Let us call this different directions of isotropization (indicated by the arrows in Fig. 2). These directions differ for betatron and Fermi accelerations. In traps with Fermi acceleration (Fig. 2a), scattering increases the number of particles in the region of large pitch angles through the decrease in their number in the region of pitch angles close to zero. In contrast, in traps with betatron acceleration, the particles escape from the region of large pitch angles and tend to fill the region of small α. It can be said that the pitch angles of the scattered particles predominantly increase for Fermi acceleration and decrease in traps with betatron acceleration compared to the collisionless case.

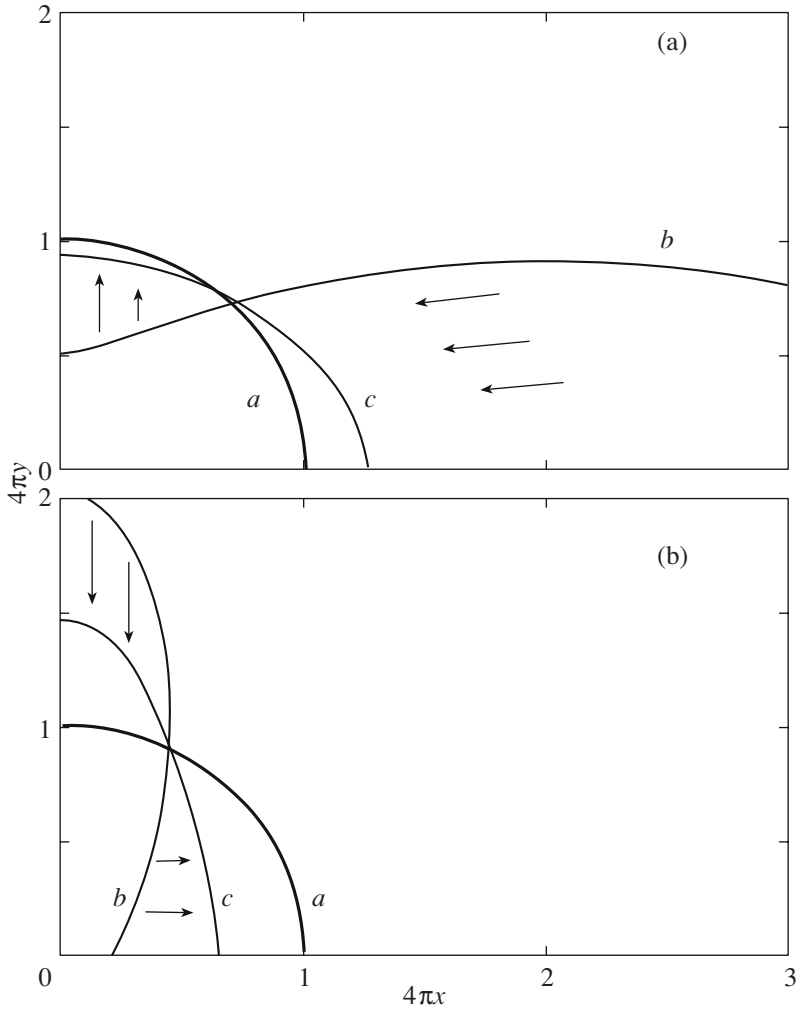

Fig. 2. Change in the pitch-angle distribution of trapped particles. (a) Fermi acceleration: *a*—initial distribution, which is assumed to be isotropic; *b*—distribution at time $l = 0.5$ in the collisionless approximation; *c*—the same distribution but with particle scattering. (b) Betatron acceleration: *a*—initial distribution; *b*—distribution at time $b = 4$ in the collisionless approximation; *c*—the same distribution with particle scattering.

The next question is the effect of Coulomb scattering on the efficiency of particle confinement in a trap. We will say that collisions increase the efficiency of particle confinement if their number inside the trap,

$$N_n = 22N_0 \int_0^{\infty} \int_{\alpha_{\rm esc}}^{\pi-\alpha_{\rm esc}} f_n(K,\alpha)\sqrt{K}dK\sin\alpha d\alpha, \quad (43)$$

increases compared to the collisionless case. If it decreases, then collisions reduce the efficiency of particle confinement. The results of the corresponding calculations are shown in Fig. 3. Curve *a* in the figure corresponds to collisionless acceleration in the trap (this case is described by Eq. (22)), while curves *b* and *c* were obtained in the approximation of weak and strong collisions. We see from their comparison that the trap confines particles most efficiently in the collisionless approximation. Even weak scattering of particles transfers some of them into the loss cone, i.e., reduces the number of particles in the trap. The stronger the scattering, the faster the particle precipitation: in the case of strong collisions (curve *c*), the number of particles N is appreciably smaller than that in the case of weak ones (curve *b*).

The particle scattering efficiency depends on the particle acceleration mechanism. At the same scattering times, traps with Fermi acceleration (Fig. 3a) confine particles better than those with betatron one. The reason is that in the case of betatron acceleration, the particles are scattered mainly in the direction of the loss cone, where they are ejected from the trap. In contrast, in traps with Fermi acceleration, the particle

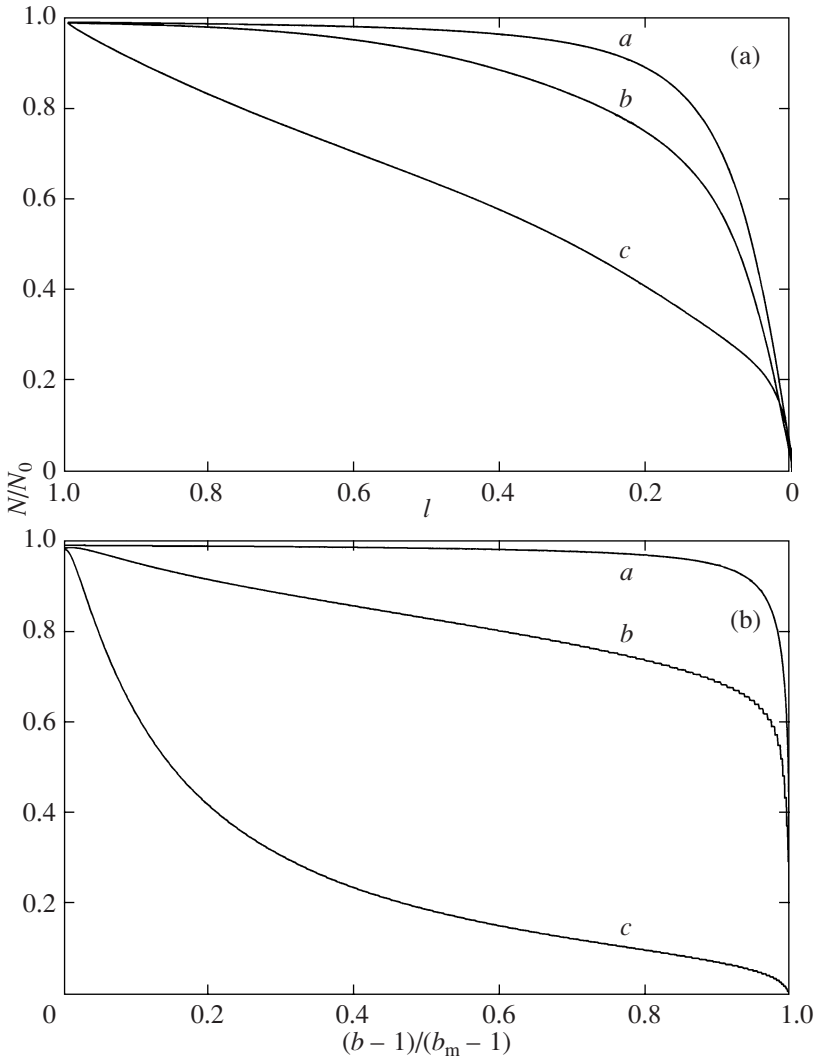

Fig. 3. Change in the number of particles in a trap: (a) Fermi acceleration and (b) betatron acceleration. Everywhere: *a*—collisionless approximation, *b*—short-lived trap with a lifetime of 10 s with particle scattering, and *c*—long-lived trap with a lifetime of 1000 s with particle scattering.

diffusion in pitch angle proceeds in a direction away from the loss cone, which increases their lifetime in the trap. Both these effects are clearly seen in Fig. 2, which shows the preferential directions of the particle diffusion in pitch angle. It can be said that the two effects (loss-cone filling and pitch-angle diffusion) collectively reduce the efficiency of particle confinement for betatron acceleration and partially cancel each other out for Fermi acceleration. As a result, a difference in the efficiencies of particle confinement in traps of different types arises.

Note that in the collisionless approximation, transversally collapsing betatron traps confine particles better than longitudinally collapsing Fermi traps. This is not true for strong scattering—a larger number of particles and their higher density can be reached in the case of Fermi acceleration.

The Coulomb interaction of particles also changes significantly their spectrum. Figure 4 shows the results of our simulation of the particle energy distribution using the formula

$$f_n(K) = 2\pi \int\limits_{\alpha_{\rm esc}}^{\pi-\alpha_{\rm esc}} f_n(K,\alpha)\sin\alpha d\alpha \qquad (44)$$

for a Maxwellian injection spectrum. Compared to the collisionless approximation, the fraction of low-

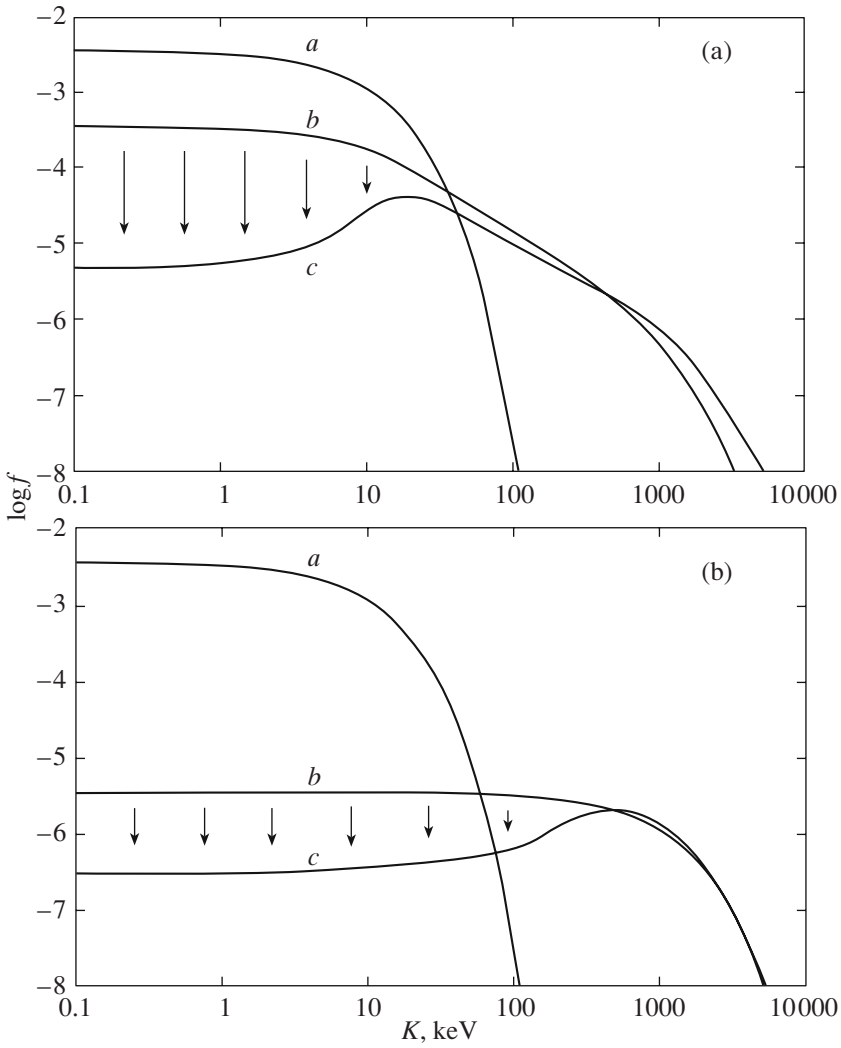

Fig. 4. Energy distribution of trapped particles: (a) Fermi acceleration and (b) betatron acceleration. Everywhere: *a*—initial particle distribution, which is assumed to be thermal with $T = 10^8$ K; *b*—final distribution in the collisionless approximation; *c*—final distribution with particle scattering.

energy particles with $K < 10$ keV, which interact with one another most efficiently and are the first to be scattered into the loss cone, decreases sharply in this distribution. In addition, the slope of the power-law segment of the spectrum decreases in traps with Fermi acceleration.

The investigation of power-law injection spectra is also significant practically. In the collisionless approximation, the shape of these spectra does not change during acceleration—the power-law distribution just shifts to the right (Bogachev and Somov 2007). If the particles interact with one another, then the power-law shape of the distribution is not retained (Fig. 5). A dip is formed in the region of low energies (P_1), because this part of the distribution escapes through the loss cone. A power-law segment with a smaller slope than that of the injection spectrum is formed in the region of energies P_2. Finally, in the region of collisionless acceleration (P_3), which corresponds to very high energies, the spectrum remains a power law with the previous slope but shifts to the right along the energy axis. As a result of these changes, the particle spectrum at energies above 10 keV becomes a double power law. Such spectra were previously detected experimentally during RHESSI observations of the Sun (see, e.g., Lin et al. 2003).

We will also present our simulation results for traps with plasma. To take into account the particle braking using (40), we must know the function $n_p(l)$, i.e., the change in plasma density as the trap col-

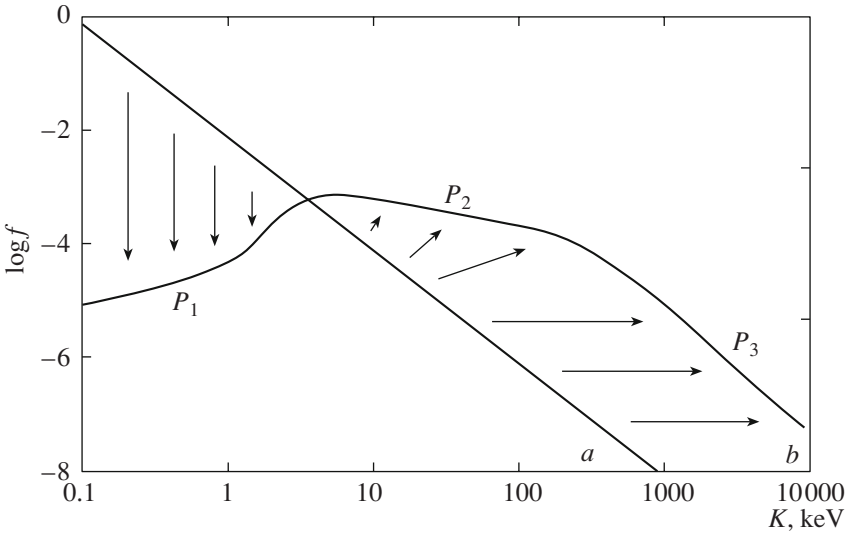

Fig. 5. Change in the power-law distribution of particles in a trap: *a*—initial particle distribution and *b*—final distribution.

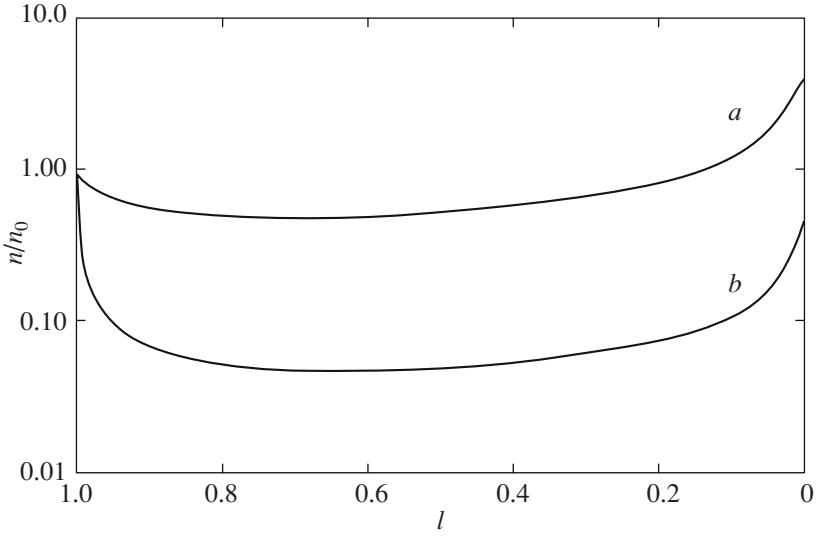

Fig. 6. Change in the plasma density in a collapsing trap: *a*—short-lived trap with a lifetime of 10 s, *b*—long-lived trap with a lifetime of 1000 s.

lapses. The results of our $n_p(l)$ simulation are shown in Fig. 6.

The plasma density in the trap changes due to the decrease in trap volume and the plasma escape through the loss cone. The former effect should lead to an increase in density, while the latter effect should lead to its decrease. Our calculations show that both these effects are roughly balanced, i.e., n_p is kept approximately at the same level throughout the acceleration process. In traps with short lifetimes, $n_p \approx n_0$, while in long-lived traps, where the scattering into the loss cone plays a greater role, $n_p \approx 0.1 n_0$, i.e., the mean density is approximately an order of magnitude lower than the initial one.

Substituting the simulated function $n_p(l)$ into Eq. (40), we will find how the simulation results will change if, apart from the particle scattering, we take into the particle braking in plasma. Our calculations showed that the presence of plasma with a density up to 10^{10} cm^{-3} in the trap affected only slightly the particle spectrum. To be more precise, this effect turned out to be negligible compared to

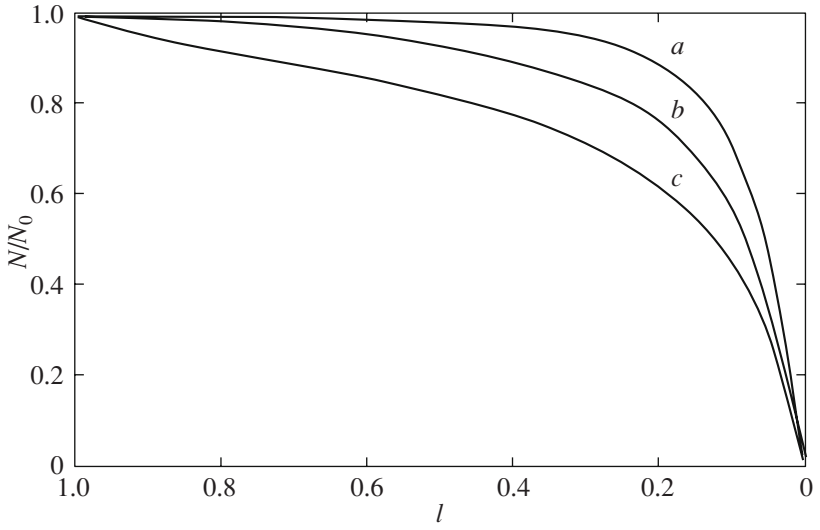

Fig. 7. Change in the number of particles in a trap: *a*—collisionless approximation, *b*—the same trap with particle scattering, *c*—the same trap with particle scattering and braking in plasma.

other factors—the acceleration of particles and their scattering due to the interaction with one another. Higher densities in the formation region of hard X-ray emission in the corona are unlikely, since these are in conflict with observations (see, e.g., Tsuneta et al. 1997).

However, we established that the plasma in the trap affects the efficiency of particle confinement. Figure 7 shows the function $N(l)$, the change in the number of particles in the trap, for three cases: (*a*) collisionless acceleration, (*b*) acceleration with particle scattering, and (*c*) acceleration with particle scattering and braking in plasma. As can be seen, in the latter case, the particles are confined least efficiently.

CONCLUSIONS

We investigated the acceleration of particles in collapsing magnetic traps in the solar corona in terms of a model that included the particle scattering and braking in plasma. Our main goal was to understand the extent to which the Coulomb interaction of particles under coronal conditions affects the efficiency of their acceleration and the shape of their spectrum. Previously, the problem of particle motion in a collapsing magnetic trap as applied to flare physics was solved only in the collisionless approximation.

To answer the question of what role is played by the Coulomb interaction, we simulated the distribution of trapped particles as a function of longitudinal and transverse trap collapse and compared the results of our calculations with those obtained in the collisionless approximation. The calculations were performed for traps of two types: collapsing traps with lifetimes of less than 10 s suggested by Somov and Kosugi (1997) and long-lived traps with lifetimes comparable to the duration of the impulsive phase of solar flares. Both types of traps can probably be formed in the corona during flares.

Our investigation showed that the Coulomb interaction of particles is weak in short-lived traps. Its characteristic times are comparable to or longer than the trap lifetime. In traps with lifetimes longer than 100–1000 s, the collisions between particles should be considered as strong ones.

From the standpoint of maximum particle energy, including the Coulomb interaction does not reduce the particle acceleration efficiency. The reason is that a coronal plasma with a density 10^8–10^9 cm^{-3}, typical of the solar corona, cannot effectively influence high-energy (50–100 keV) particles and the acceleration of the latter is virtually collisionless. The particle spectra in the corresponding energy range are described with a high accuracy by the formulas derived in the collisionless approximation (Bogachev and Somov 2007).

At energies below 10 keV, the interaction of particles is strong. A dip produced by the braking of this part of the distribution in plasma and by the effective scattering of low-energy particles into the loss cone is formed in the particle distributions in this energy range.

Including the Coulomb interaction reduces the efficiency of particle confinement in traps. The largest and smallest numbers of particles are reached, respectively, in collisionless traps and in long-lived

traps with effective particle scattering and braking. Nevertheless, even in the latter case, collapsing traps are capable of confining more than 20% of the injected particles for a long time (up to half of their lifetime). This percentage exceeds 80% for short-lived traps and 90% for traps with collisionless acceleration.

The efficiency of particle confinement also depends on the predominant acceleration mechanism, the betatron or Fermi one. In the collisionless approximation, the particles are better confined in traps with betatron acceleration. This is not true when the scattering is taken into account—a larger number of particles and their higher density are reached in the case of Fermi acceleration.

The interaction of particles with one another and with plasma causes changes in their spectra that can be detected through observations. A double-power-law spectrum with an inflection point at energies above 10 keV is formed for a power-law spectrum of particle injection from the reconnection region inside traps. Such spectra were previously detected experimentally during RHESSI measurements of the hard X-ray emission from coronal sources. Our model explains these observations.

REFERENCES

1. M. J. Aschwanden, *Particle Acceleration and Kinematics in Solar Flares* (Kluwer Academ. Publ., Dordrecht, 2002).
2. S. A. Bogachev and B. V. Somov, Astron. Zh. **78**, 187 (2001) [Astron. Rep. **45**, 157 (2001)].
3. S. A. Bogachev and B. V. Somov, Pis'ma Astron. Zh. **31**, 601 (2005) [Astron. Lett. **31**, 537 (2005)].
4. S. A. Bogachev and B. V. Somov, Pis'ma Astron. Zh. **33**, 62 (2007) [Astron. Lett. **33**, 54 (2007)].
5. J. C. Brown and P. Hoyng, Astrophys. J. **200**, 734 (1975).
6. A. M. Bykov, R. A. Chevalier, D. C. Ellison, et al., Astrophys. J. **538**, 203 (2000).
7. P. Giuliani, T. Neukirch, and P. Wood, Astrophys. J. **635**, 636 (2005).
8. M. Karlicky and T. Kosugi, Astron. Astrophys. **419**, 1159 (2004).
9. A. A. Korchak, Solar Phys. **66**, 149 (1980).
10. V. A. Kovalev and B. V. Somov, Pis'ma Astron. Zh. **29**, 465 (2003) [Astron. Lett. **29**, 409 (2003)].
11. L. I. Miroshnichenko, *Solar Cosmic Rays* (Kluwer Academ. Publ., Dordrecht, 2001).
12. R. P. Lin, S. Krucker, G. D. Holman, et al. Proc. 28th Int. Cosmic Ray Conf. 3207 (2003).
13. B. V. Somov, *Plasma Astrophysics, Part I, Fundamentals and Practice* (Springer, New York, 2006a).
14. B. V. Somov, *Plasma Astrophysics, Part II, Reconnection and Flares* (Springer, New York, 2006b).
15. B. V. Somov and T. Kosugi, Astrophys. J. **485**, 859 (1997).
16. B. V. Somov and S. A. Bogachev, Pis'ma Astron. Zh. **29**, 701 (2003) [Astron. Lett. **29**, 621 (2003)].
17. B. V. Somov, J.-C. Hénoux, and S. A. Bogachev, Adv. Space Res. **30**, 55 (2002).
18. S. Tsuneta, S. Masuda, T. Kosugi, and J. Sato, Astrophys. J. **478**, 787 (1997).

Translated by V. Astakhov